

Designing Sparse Sensing Matrices for Image Compression

Tao Hong, Xiao Li, Zihui Zhu, and Qiuwei Li

Abstract—We consider designing a sparse sensing matrix which contains few non-zero entries per row and can be efficiently applied for capturing signals. The optimal sparse sensing matrix is designed so that it is also robust to sparse representation error of the signals and the Gram matrix of the equivalent dictionary is as close as possible to a target Gram matrix with small mutual coherence. An alternating minimization-based algorithm is proposed for solving the optimal design problem. We provide convergence analysis of the proposed algorithm which is proved to have sequence convergence, i.e., it generates a sequence that converges to a stationary point of the minimization problem. Experimental results show that the obtained sparse sensing matrix (even each row is extremely sparse) significantly outperforms a random dense sensing matrix in terms of signal reconstruction accuracy of synthetic data and peak signal-to-noise ratio (PSNR) for real images.

Index Terms—Compressive sensing, mutual coherence, structured sensing matrix, sequence convergence.

I. INTRODUCTION

Compressive sensing (CS)—that aims to break through the Shannon-Nyquist limit for sampling signals—has attracted great attention since it was introduced a little more than a decade ago [1]–[4]. The performance of a CS system strongly depends on two ingredients: a *sensing matrix* $\Phi \in \mathbb{R}^{M \times N}$ (where $M \ll N$) which compresses a signal \mathbf{x} via $\mathbf{y} = \Phi \mathbf{x}$ and a *dictionary* $\Psi \in \mathbb{R}^{N \times L}$ (where $L \geq N$) that captures the concise structure of the signal. In particular, we say $\mathbf{x} \in \mathbb{R}^N$ is sparse (in Ψ) if we can (approximately) represent \mathbf{x} with a few columns (also referred to as atoms) from Ψ :

$$\mathbf{x} = \Psi \mathbf{s} + \mathbf{e} = \sum_{\ell} \Psi(:, \ell) \mathbf{s}(\ell) + \mathbf{e} \quad (1)$$

where $\|\mathbf{s}\|_0 \leq K$ with $K \ll L$.¹ Here \mathbf{e} is referred to as the sparse representation error (SRE) vector of \mathbf{x} under Ψ . We say \mathbf{x} is exactly sparse in Ψ if \mathbf{e} is nil.

The choice of dictionary Ψ depends on the signal model and traditionally we attempt to concisely capture the structure contained in the signals of interest by a well-designed

This research is supported in part by ERC Grant agreement no. 320649, and in part by the Intel Collaborative Research Institute for Computational Intelligence (ICRI-CI).

T. Hong is with Department of Computer Science, Technion - Israel Institute of Technology, Haifa, 32000, Israel (e-mail: hongtao@cs.technion.ac.il).

X. Li is with Department of Electronic Engineering, The Chinese University of Hong Kong, Shatin, NT, Hong Kong (e-mail: xli@ee.cuhk.edu.hk).

Z. Zhu and Q. Li are with Department of Electrical Engineering, Colorado School of Mines, Golden, CO 80401 USA (e-mail: {zzhu,quli}@mines.edu).

¹Throughout this paper, MATLAB notations are adopted: $\mathbf{Q}(m, :)$, $\mathbf{Q}(:, k)$ and $\mathbf{Q}(i, j)$ denote the m th row, k th column, and (i, j) th entry of the matrix \mathbf{Q} ; $\mathbf{q}(n)$ denotes the n -th entry of the vector \mathbf{q} . $\|\cdot\|_0$ is used to count the number of nonzero elements.

dictionary. Typical examples include the Fourier matrix for frequency-sparse signals, and a multiband modulated Discrete Prolate Spheroidal Sequences (DPSS's) dictionary for sampled multiband signals [5]. Dictionary learning is another popular approach that learns a dictionary by giving a set of representative signals (called training data) [6]–[8].

As we mentioned before another important factor in CS is to choose an appropriate sensing matrix Φ preserving the useful information contained in the signal \mathbf{x} such that it is possible to recover \mathbf{x} from its low dimensional measurement $\mathbf{y} = \Phi \mathbf{x}$. It has been shown that if the *equivalent dictionary* $\Phi \Psi$ satisfies the restricted isometry property (RIP), a sparse signal can be exactly reconstructed from its linear measurement \mathbf{y} [1], [9]. Despite the fact that a random matrix satisfies the RIP with high probability [9], testing whether a matrix satisfies the RIP is NP-hard [10]. Therefore, mutual coherence—another measure of the sensing matrices that is much easier to verify—has been alternatively utilized as a guideline to design the sensing matrix [11]–[17].

In hardware implementation [18] and applications like electrocardiography (ECG) compression [19] and data stream computing [20], the complexity for sampling signals is of significant importance. For example, in designing hardware system, it is known that more CPU clocks and Power are required for the multiplication unit compared with other units (such as addition unit). Due to such concerns, it is crucial to consider the computational complexity of sensing matrices for practical applications. One natural and effective strategy for decreasing the number of multiplying units and reducing the computational complexity of acquiring signals is designing a sparse sensing matrix Φ , which contains very few non-zero elements per row. Such a sparse sensing matrix can be efficiently utilized for capturing signals. In addition, the utility of a sparse sensing matrix is also useful for developing efficient algorithms, as we note that a set of iterative methods for sparse linear systems require performing the sensing matrix to a vector (which is usually called residual) in each iteration. We refer the reader to [20] for more applications where a sparse sensing matrix is useful and also crucial. To the best of our knowledge, this is the first work to design a sparse sensing matrix via enhancing the mutual coherence property of the equivalent dictionary. The main contributions are stated as follows:

- The first contribution is to propose a framework for designing a (structured) sparse sensing matrix based on decreasing the mutual coherence of the equivalent dictionary and the resulted sensing matrix is also robust to SRE, which is generally not negligible in practical

applications like image processing [15].

- The second contribution is to provide an alternating minimization-based algorithm for solving the optimal design problem. We note that alternating minimization-based algorithm has been popularly utilized in designing sensing matrix [11]–[16], in which the convergence of the algorithms is usually neither ensured nor seriously considered. Following this concern, the convergence analysis of the proposed algorithm is provided in this paper. In particular, we show the proposed algorithm generates a sequence that converges to a stationary point of the minimization problem.

The outline of this paper is given as follows. We review the previous approach for robust sensing matrix in Section II. In Section III, we propose a framework for designing a (structured) sparse sensing matrix by considering the mutual coherence behavior of the equivalent dictionary as well as sparse representation errors of the signals. An alternating minimization-based algorithm for solving the optimal design problem is provided in Section IV. We demonstrate the performance of the obtained sparse sensing matrix with experiments on synthetic data and real images in Section V. Some conclusions are given in Section VI to end this paper.

II. PRELIMINARY

A. Mutual Coherence

To begin, we briefly relate the concept of mutual coherence to CS. The *mutual coherence* of $\mathbf{Q} \in \mathbb{R}^{M \times L}$ is defined as

$$\mu(\mathbf{Q}) \triangleq \max_{1 \leq i \neq j \leq L} \frac{|\mathbf{q}_i^T \mathbf{q}_j|}{\|\mathbf{q}_i\|_2 \|\mathbf{q}_j\|_2} \geq \underline{\mu} \triangleq \sqrt{\frac{L-M}{M(L-1)}} \quad (2)$$

where \mathbf{q}_i is the i -th column of \mathbf{Q} and $\underline{\mu}$ is the lower bound of the mutual coherence of \mathbf{Q} , i.e., Welch Bound [21].

With the projected measurement \mathbf{y} of the form

$$\mathbf{y} = \bar{\Phi} \mathbf{x} \quad (3)$$

and the prior information that \mathbf{x} is sparse in $\bar{\Psi}$, we can recover the signal as $\hat{\mathbf{s}} = \bar{\Psi} \hat{\mathbf{s}}$ where²

$$\begin{aligned} \hat{\mathbf{s}} &= \arg \min \|\mathbf{y} - \bar{\Phi} \bar{\Psi} \mathbf{s}\|_2^2 \\ \text{s.t. } &\|\mathbf{s}\|_0 \leq K \end{aligned} \quad (4)$$

which can be exactly or approximately solved via convex methods [1], [22], [23] or greedy algorithm [24], like the orthogonal marching pursuit (OMP). It is shown in [24] that OMP can stably solve (4) (and hence obtain accurate estimation of \mathbf{x}) if

$$K < \frac{1}{2} \left[1 + \frac{1}{\mu(\bar{\Phi} \bar{\Psi})} \right] \quad (5)$$

where $\bar{\Phi} \bar{\Psi}$ is referred to as the equivalent dictionary of the CS system. This is a simple motivation of designing a sensing matrix with small mutual coherence $\mu(\bar{\Phi} \bar{\Psi})$ as it enables a large set of sparse signals that can be recovered from the projected measurement. We refer the reader to [11], [14] and the references therein for more discussions.

²Here $\|\cdot\|_2$ is used to denote the l_2 norm for a vector.

B. Optimized Robust Sensing Matrix [15], [16]

Motivated by (5), the sensing matrices in [11], [13], [14] are obtained via minimizing the mutual coherence $\mu(\bar{\Phi} \bar{\Psi})$. The equivalent dictionary with the optimized sensing matrix has small mutual coherence and the corresponding CS system yields better performance than the one with a random sensing matrix for the exactly sparse signals (i.e., $\mathbf{e} = \mathbf{0}$ for the signal model (1)). However, it was recently realized that such a sensing matrix is not robust to SRE in (1) (for example it exists when we represent the real images with a learned dictionary) and thus the corresponding CS system yields poor performance, especially in image processing [15]. Let $\mathbf{X} \in \mathbb{R}^{N \times J}$ be a set of training data and \mathbf{S} consists of the sparse coefficients of \mathbf{X} in $\bar{\Psi}$: $\mathbf{X} = \bar{\Psi} \mathbf{S} + \mathbf{E}$ where $\|\mathbf{S}(:, j)\|_0 \leq K, \forall j$. Then, in [15], [16], the SRE matrix

$$\mathbf{E} := \mathbf{X} - \bar{\Psi} \mathbf{S} \quad (6)$$

is utilized to design a sensing matrix which is robust to SRE.

Denote by \mathcal{G}_ξ the set of relaxed equiangular tight frame (ETF) Gram matrices:

$$\mathcal{G}_\xi = \left\{ \mathbf{G} \in \mathbb{R}^{L \times L} : \mathbf{G}(i, i) = 1, \forall i, \max_{i \neq j} |\mathbf{G}(i, j)| \leq \xi \right\} \quad (7)$$

where $\xi \in [0, 1)$ is a pre-set threshold and is usually chosen as 0 or $\underline{\mu}$. Note that when $\xi = 0$, $\mathcal{G}_\xi = \{\mathbf{I}\}$ only contains the identity matrix. $\xi = \underline{\mu}$ is also popularly utilized in [13]–[16].

The sensing matrices proposed in [15], [16] are optimized by solving the following problem³:

$$\min_{\Phi, G \in \mathcal{G}_\xi} \|\mathbf{G} - \bar{\Psi}^T \bar{\Phi}^T \bar{\Phi} \bar{\Psi}\|_F^2 + \lambda \|\bar{\Phi} \mathbf{E}\|_F^2 \quad (8)$$

where the first term is utilized to minimize the mutual coherence of the equivalent dictionary, the second term $\|\bar{\Phi} \mathbf{E}\|_F^2$ is utilized to make the sensing matrix robust to SRE, and $\lambda \geq 0$ is the trade-off parameter to balance the mutual coherence of the equivalent dictionary and robustness of the sensing matrix to the SRE. Simulations have shown that the designed sensing matrices by (8) achieves the state-of-the-art performance for CS-based image compression [15].

III. OPTIMIZED SPARSE SENSING MATRIX

In this section, we consider designing a (structured) sparse sensing matrix by considering the SRE of the signals and the mutual coherence of the equivalent dictionary.

As explained before, in applications like ECG compression [19], data stream computing [20] and hardware implementation [18], the classical CS system with a dense sensing matrix $\bar{\Phi}$ encounters computational issues. Indeed, merely applying a sensing matrix $\bar{\Phi} \in \mathbb{R}^{M \times N}$ to capture a length- N signal has the computational complexity of $O(MN)$, which is prohibitive when N is large. In applications like image processing, one often partitions the image into a set of patches of small size (like 8×8 patches) to make the problem computationally tractable. However, the recent work in dictionary learning [25] and sensing matrix design [17] has

³ $\|\cdot\|_F$ represents the Frobenius norm.

revealed that larger-size patches (like 64×64 patches) lead to better performance for image processing like image denoising and image compression.

An approach to tackle this computational difficulties is to incorporate some certain structures into the sensing matrix Φ . One of such structure is the (structured) sparse sensing matrix where the sensing matrix consists of a sparse matrix and a structured matrix that both can be efficiently applied to a vector:

$$\Phi = \tilde{\Phi} A, \quad (9)$$

where $A \in \mathbb{R}^{N \times N}$ is referred to as a *base sensing matrix* and $\tilde{\Phi} \in \mathbb{R}^{M \times N}$ is a row-wise sparse matrix that can be designed by certain criteria. The structured matrix A is often an orthonormal matrix and can be efficiently applied to a length- N vector. Typical choices of A include the DCT matrix and Walsh-Hadamard matrix both of which can be applied to a length- N vector in $O(N \log N)$. Usually the choice of A depends on specific applications. For example, the DCT matrix has been demonstrated to be useful in image processing [26]. We show that the DCT matrix can improve the image reconstruction accuracy compared with the one without the DCT matrix when the matrix Φ is very sparse in Section V. Note that we can rewrite

$$\bar{\Phi}^T = A^T \tilde{\Phi}^T \quad (10)$$

and view $\bar{\Phi}^T$ as the sparse representation of Φ^T in A . Thus, throughout this paper, similar to (1) where we call x is sparse (in $\bar{\Phi}$) though itself is not sparse, we also say $\bar{\Phi}$ in (9) a sparse sensing matrix (in A). Similar form to (10) appears in double-sparsity dictionary [26], where the dictionary $\bar{\Psi} = A \bar{\Phi}$ with $\bar{\Psi}$ an overcomplete but column-wise sparse dictionary learned from the training data.

Before presenting the sparse sensing matrix design problem, we note that one drawback of the approach in [15], [16] is that the SRE matrix E (defined in (6)) depends on the training data X which is very large or requires extra effort to obtain in some applications, like image processing with a wavelet dictionary which is not learned from data. To get rid of the dependence of the training data X and SRE matrix E , let us model each column of E as an independently and identically distributed (i.i.d.) Gaussian random vector of mean zero and covariance $\sigma^2 \mathbf{I}$. Then $\frac{\|\Phi E\|_F^2}{J}$ converges in probability and almost surely to $\sigma^2 \|\Phi\|_F^2$ when the number of training samples J approaches to ∞ [17]. Thus minimizing $\|\Phi\|_F$ is also expected to result in a sensing matrix that is robust to the SRE of the signals.

Now it is clear that our goal is to design a sensing matrix $\bar{\Phi} = \tilde{\Phi} A$ such that it is robust to the SRE of the signals and the resulting equivalent dictionary $\bar{\Phi} \bar{\Psi}$ also has small mutual coherence. We design the sparse sensing matrix via

$$\begin{aligned} \{\tilde{\Phi}, \bar{G}\} = \operatorname{argmin}_{\Phi, G \in \mathcal{G}_\xi} & \|G - \bar{\Psi}^T A^T \Phi^T \Phi A \bar{\Psi}\|_F^2 + \lambda \|\Phi A\|_F^2 \\ \text{s.t. } & \|\Phi(m, :)\|_0 \leq \kappa, \forall m, \end{aligned} \quad (11)$$

where $\lambda \geq 0$ is utilized to balance the mutual coherence of the equivalent dictionary and robustness of the sensing matrix to the SRE. A few remarks are given as follows.

Remark 3.1:

- As we stated before, we usually choose $A \in \mathbb{R}^{N \times N}$ as the one that can be applied to a vector with complexity at most $O(N \log N)$.⁴ Thus, the total computational complexity of $\bar{\Phi}x = \tilde{\Phi}Ax$ is $O(N \log N + M\kappa)$. When A is the identity matrix, then $\bar{\Phi} = \tilde{\Phi}$ and the corresponding complexity reduces to $O(M\kappa)$. This is a significant reduction of computational complexity compared with a dense sensing matrix which requires $O(MN)$ computational complexity to sense a signal.
- Replacing the term $\|\Phi E\|_F^2$ in (8) by $\|\Phi\|_F^2$ has also been suggested in [17]. Experiments with real images demonstrated that the designed sensing matrix in [17] has similar or slightly better performance than the one obtained in [15], [16].
- The set of Gram matrices \mathcal{G}_ξ is defined in (7). The parameter $\xi \in [0, 1]$ is a pre-set threshold and is usually chosen as 0 or $\underline{\mu}$ (defined in (2)). We note that $\xi = \underline{\mu}$ is suggested to design a sensing matrix for the exactly sparse signals, while $\xi = 0$ (i.e., $\mathcal{G}_\xi = \{\mathbf{I}\}$) is recommended for optimizing a sensing matrix that is utilized when SRE exists, like in image processing [15]–[17].
- Aside from the facts that $\bar{\Phi}$ is parameterized by $\tilde{\Phi}A$, (11) differs from (8) in that the former has a sparse constraints on the rows of the sensing matrix $\tilde{\Phi}$. However, this sparse constraint makes (11) highly nonconvex. We will propose an algorithm to address this constraint and then solve (11) in next section.

IV. PROPOSED ALGORITHM FOR DESIGNING SPARSE SENSING MATRIX

In this section, we provide an alternating minimization-based algorithm for solving the sparse sensing matrix design problem (11). We also provide rigorous convergence analysis of the proposed algorithm.

A. Proposed Algorithm for Designing Sparse Sensing Matrix

To begin, suppose A is an $N \times N$ orthonormal basis and we rewrite (11) as

$$\begin{aligned} \min_{\Phi, G} f(\Phi, G) = & \|G - \bar{\Psi}^T \Phi^T \Phi \bar{\Psi}\|_F^2 + \lambda \|\Phi\|_F^2 \\ \text{s.t. } & \|\Phi(m, :)\|_0 \leq \kappa, \forall m, G \in \mathcal{G}_\xi \end{aligned} \quad (12)$$

where $\bar{\Psi} = A \bar{\Phi}$. Let $\mathcal{P}_{\mathcal{G}_\xi} : \mathbb{R}^{L \times L} \rightarrow \mathbb{R}^{L \times L}$ denote an orthogonal projector onto the set \mathcal{G}_ξ :

$$(\mathcal{P}_{\mathcal{G}_\xi}(G))(i, j) = \begin{cases} 1, & i = j, \\ \operatorname{sign}(G(i, j)) \min(|G(i, j)|, \xi), & i \neq j. \end{cases}$$

First note that the solution of minimizing f in terms of G when Φ is fixed is given by

$$\hat{G} = \operatorname{argmin}_{G \in \mathcal{G}_\xi} f(\Phi, G) = \mathcal{P}_{\mathcal{G}_\xi}(\bar{\Psi}^T \Phi^T \Phi \bar{\Psi}). \quad (13)$$

⁴In some cases, such a matrix A can be implemented with complexity $O(N)$. For example, if we utilize the DCT matrix and decompose it into a series of Givens rotation matrices [27], it has computational complexity $O(N)$ [27].

Now we consider solving (12) in terms of Φ when G is fixed:

$$\min_{\Phi} f(\Phi, G) \quad \text{s.t. } \|\Phi(m, :)\|_0 \leq \kappa, \quad \forall m. \quad (14)$$

Without the sparsity constraint, the recent works [28], [29] have shown that a number of iterative algorithms (including gradient descent) can provably solve $\min_{\Phi} f(\Phi, G)$.⁵ Thus, with the sparsity constraint in (14), we utilize the projected gradient descent (PGD) to solve (14). The gradient of $f(\Phi, G)$ in terms of Φ is given as follows:

$$\nabla_{\Phi} f(\Phi, G) = 2\lambda\Phi - 4\Phi\Psi G\Psi^T + 4\Phi\Psi\Psi^T\Phi^T\Phi\Psi\Psi^T. \quad (15)$$

For convenience, we let \mathcal{S}_κ denote the set of matrices whose rows have at most κ non-zero elements:

$$\mathcal{S}_\kappa \triangleq \{Z \in \mathbb{R}^{M \times N} : \|Z(m, :)\|_0 \leq \kappa, \quad \forall m\}.$$

We denote $\mathcal{P}_{\mathcal{S}_\kappa} : \mathbb{R}^{M \times N} \rightarrow \mathbb{R}^{M \times N}$ as an orthogonal projector onto the set of \mathcal{S}_κ : for any $M \times N$ input matrix, it keeps the κ components of each row with the largest absolute value.⁶

Then, in the k -th step, we update Φ as

$$\Phi_k = \mathcal{P}_{\mathcal{S}_\kappa}(\Phi_{k-1} - \eta \nabla f(\Phi_{k-1}, G_{k-1})). \quad (16)$$

We summarize the alternating minimization-based algorithm for solving (12) in Algorithm 1.⁷ Note that alternating minimization-based algorithm has been popularly utilized for designing sensing matrix [11]–[16]. However, the convergence of these algorithms is usually neither ensured nor seriously considered. In next section, we provide the rigorous convergence analysis for the proposed Algorithm 1.

Algorithm 1 Algorithm for Designing Sparse Sensing Matrix Initialization:

Initial value Φ_0 , the number of maximal iterations $Iter_{max}$, step size η , the sparsity level κ and the given trade-off parameter λ .

Output:

Sparse sensing matrix $\Phi_{Iter_{max}}$.

- 1: $k \leftarrow 1$
- 2: **while** $k \leq Iter_{max}$ **do**
- 3: Update Φ : $\Phi_k \in \mathcal{P}_{\mathcal{S}_\kappa}(\Phi_{k-1} - \eta \nabla f(\Phi_{k-1}, G_{k-1}))$
- 4: Update G : $G_k = \mathcal{P}_{\mathcal{G}_\xi}(\Psi^T \Phi_k^T \Phi_k \Psi)$
- 5: $k \leftarrow k + 1$
- 6: **end while**

B. Convergence Analysis

We now examine the convergence of Algorithm 1. To this end, we first transfer (17) into the following unconstrained problem

$$\min_{\Phi, G} \rho(\Phi, G) := f(\Phi, G) + \delta_{\mathcal{S}_\kappa}(\Phi) + \delta_{\mathcal{G}_\xi}(G), \quad (17)$$

⁵This is also numerically verified in [17].

⁶If there exist more than one choice to the κ largest components, we pick any one of them.

⁷We can either pick the initialization Φ_0 as a random matrix, or the one given in [14, Theorem 2].

where $\delta_{\mathcal{S}_\kappa}(\Phi) = \begin{cases} 0, & \Phi \in \mathcal{S}_\kappa, \\ \infty, & \Phi \notin \mathcal{S}_\kappa \end{cases}$ is the indicator function (and similarly for $\delta_{\mathcal{G}_\xi}(G)$). It is clear that (17) is equivalent to the original constrained problem (12). We note that the reason we consider the unconstrained one (17) because it is easier to have notions like stationary points for (17) than for the constrained counterpart (12).

Note that by updating G with (13), $\rho(\Phi_k, G_k) \leq \rho(\Phi_k, G_{k-1})$.⁸ We also need to show the objective function is decreasing by updating the sensing matrix Φ . To that end, we let $\rho_0 = \rho(\Phi_0, G_0)$ and consider the sublevel set of ρ :

$$\mathcal{L}_{\rho_0} = \{(\Phi, G) : \rho(\Phi, G) \leq \rho_0, G \in \mathcal{G}_\xi, \Phi \in \mathcal{S}_\kappa\}.$$

It is clear that for any point $(\Phi, G) \in \mathcal{L}_{\rho_0}$, $\|G\|_F$ is finite since $G \in \mathcal{G}_\xi$ and $\|\Phi\|_F$ is finite since $\rho \rightarrow \infty$ when $\|\Phi\|_F \rightarrow \infty$. Then with simple calculation, we have that both $\nabla_{\Phi} f(\Phi, G)$ and $\nabla_G f(\Phi, G)$ are Lipschitz continuous for all $(\Phi, G) \in \mathcal{L}_{\rho_0}$, i.e.,

$$\begin{aligned} \|\nabla_{\Phi} f(\Phi, G) - \nabla_{\Phi} f(\Phi', G)\|_F &\leq L_c \|\Phi - \Phi'\|_F \\ \|\nabla_G f(\Phi, G) - \nabla_G f(\Phi, G')\|_F &\leq L_c \|G - G'\|_F \end{aligned} \quad (18)$$

for all $(\Phi, G), (\Phi', G), (\Phi, G') \in \mathcal{L}_{\rho_0}$. Here $L_c > 0$ is the Lipschitz constant. A direct consequence of the Lipschitz gradient is as follows.

Lemma 1. *For any $L \geq L_c$, denote by*

$$\begin{aligned} h_L(\Phi, \Phi', G) := & f(\Phi', G) + \langle \nabla_{\Phi} f(\Phi', G), \Phi - \Phi' \rangle \\ & + \frac{L}{2} \|\Phi - \Phi'\|_F^2. \end{aligned}$$

Then,

$$f(\Phi, G) \leq h_L(\Phi, \Phi', G)$$

for all $(\Phi, G) \in \mathcal{L}_{\rho_0}$ and $(\Phi', G) \in \mathcal{L}_{\rho_0}$.

Proof. We parametrize the function value through the line passing $[\Phi', \Phi]$ by t , i.e., define $v(t) = f(\Phi' + t(\Phi - \Phi'), G)$. It is clear that $v(0) = f(\Phi', G)$, $v(1) = f(\Phi, G)$. Then we have

$$\begin{aligned} v(1) - v(0) &= f(\Phi, G) - f(\Phi', G) = \int_0^1 v'(t) dt \\ &= \int_0^1 \langle \nabla_{\Phi} f(\Phi' + t(\Phi - \Phi'), G), \Phi - \Phi' \rangle dt \\ &= \int_0^1 \langle \nabla_{\Phi} f(\Phi' + t(\Phi - \Phi'), G) - \nabla_{\Phi} f(\Phi', G), \Phi - \Phi' \rangle dt \\ &\quad + \langle \nabla_{\Phi} f(\Phi', G), \Phi - \Phi' \rangle \\ &\leq \int_0^1 \|\nabla_{\Phi} f(\Phi' + t(\Phi - \Phi'), G) - \nabla_{\Phi} f(\Phi', G)\|_F dt \\ &\quad \cdot \|\Phi - \Phi'\|_F + \langle \nabla_{\Phi} f(\Phi', G), \Phi - \Phi' \rangle \\ &\leq L \|\Phi - \Phi'\|_F^2 \int_0^1 t dt + \langle \nabla_{\Phi} f(\Phi', G), \Phi - \Phi' \rangle \\ &= \frac{L}{2} \|\Phi - \Phi'\|_F^2 + \langle \nabla_{\Phi} f(\Phi', G), \Phi - \Phi' \rangle, \end{aligned}$$

where in the last inequality we have used (18). \square

⁸This inequality is shown in Appendix A.

With Lemma 1, we first establish that the sequence generated by Algorithm 1 is bounded and the limit point of any its convergent subsequence is a stationary point of ρ .

Theorem 1 (Subsequence convergence). *Let $\{\mathbf{W}_k\}_{k \geq 0} = \{(\Phi_k, \mathbf{G}_k)\}_{k \geq 0}$ be the sequence generated by Algorithm 1 with a constant step size $\eta < \frac{1}{L_c}$. Then the sequence $\{(\Phi_k, \mathbf{G}_k)\}_{k \geq 0}$ is bounded and obeys the following properties:*

(P1) *sufficient decrease:*

$$\begin{aligned} \rho(\mathbf{W}_k) - \rho(\Phi_{k+1}, \mathbf{G}_k) &\geq \frac{\frac{1}{\eta} - L_c}{2} \|\Phi_k - \Phi_{k+1}\|_F^2, \\ \rho(\Phi_{k+1}, \mathbf{G}_k) - \rho(\mathbf{W}_{k+1}) &\geq \|\mathbf{G}_k - \mathbf{G}_{k+1}\|_F^2. \end{aligned} \quad (19)$$

(P2) *the sequence $\{\rho(\Phi_k, \mathbf{G}_k)\}_{k \geq 0}$ is convergent.*

(P3) *convergent difference:*

$$\lim_{k \rightarrow \infty} \|\mathbf{W}^{k+1} - \mathbf{W}^k\|_F = 0. \quad (20)$$

(P4) *for any convergent subsequence $\{\mathbf{W}_{k'}\}$, its limit point $\underline{\mathbf{W}}$ is a stationary point of ρ and*

$$\lim_{k' \rightarrow \infty} \rho(\mathbf{W}_{k'}) = \lim_{k \rightarrow \infty} \rho(\mathbf{W}_k) = \rho(\underline{\mathbf{W}}). \quad (21)$$

The proof of theorem 1 is given in Appendix A. In a nutshell, theorem 1 implies that the sequence generated by Algorithm 1 has at least one convergent subsequence, and the limit point of any convergent subsequence is a stationary point of ρ . The following result establishes that the sequence generated by Algorithm 1 is a Cauchy sequence and thus the sequence itself is convergent and converges to a stationary point of ρ .

Theorem 2 (Sequence convergence). *The sequence $\{(\Phi_k, \mathbf{G}_k)\}_{k \geq 0}$ generated by Algorithm 1 with a constant step size $\eta < \frac{1}{L_c}$ converges to a stationary point of ρ .*

The proof of Theorem 2 is given in Appendix B. A special property named Kurdyka-Łojasiewicz (KL) inequality (see Definition 2 in Appendix B) of the objective function is introduced in proving Theorem 2. We note that the KL inequality has been utilized to prove the convergence of proximal alternating minimization algorithms [30]–[32]. Our proposed Algorithm 1 differs from the proximal alternating minimization algorithms [30]–[32] in that we update \mathbf{G} (see (13)) by exactly minimizing the objective function rather than utilizing a proximal operator (which decreases the objective function less than the one by exactly minimizing the objective function). Updating \mathbf{G} by exactly minimizing the objective function is popularly utilized in [11]–[16]. We believe our proof techniques for Theorems 1 and 2 will also be useful to analyze the convergence of other algorithms for designing sensing matrices [11]–[16].

In terms of the step size for updating Φ , Algorithm 1 utilizes a simple constant step size to simplify the analysis. But we note that the convergence analysis in theorem 1 and theorem 2 can also be established for adaptive step size. In particular, in Appendix C, we provide a backtracking method to choose the step sizes, which should be useful for practical

implementation, especially when it is not easy to compute the Lipschitz constant L_c .

When $\xi = 0$, \mathcal{G}_ξ consists of a single element (i.e., $\mathcal{G}_\xi = \{\mathbf{I}\}$) and the problem (17) is equivalent to

$$\min_{\Phi} \nu(\Phi) := \|\mathbf{I} - \Psi^T \Phi^T \Psi \Phi\|_F^2 + \lambda \|\Phi\|_F^2 + \delta_{\mathcal{S}_\kappa}(\Phi). \quad (22)$$

Then, Algorithm 1 reduces to the projected gradient descent (PGD), which is known as the iterative hard thresholding (IHT) algorithm for compressive sensing [33]. As a direct consequence of Theorems 1 and 2, the following result establishes convergence analysis of PGD for solving (22).

Corollary 1. *Let $\{\Phi_k\}_{k \geq 0}$ be the sequence generated by the PGD method with a constant step size $\eta < \frac{1}{L_c}$:*

$$\Phi_{k+1} = \mathcal{P}_{\mathcal{S}_\kappa}(\Phi_k - \eta \nabla_{\Phi} f(\Phi_k, \mathbf{I})),$$

where $\nabla_{\Phi} f(\Phi_k, \mathbf{I})$ is given in (15). Then

- $\nu(\Phi_k) - \nu(\Phi_{k+1}) \geq \frac{\frac{1}{\eta} - L_c}{2} \|\Phi_k - \Phi_{k+1}\|_F^2$
- the sequence $\{\nu(\Phi_k)\}_{k \geq 0}$ converges.
- the sequence $\{\Phi_k\}$ converges to a stationary point of ν .

We note that Corollary 1 can also be established for PGD solving general sparsity-constrained problem if the objective function has Lipschitz gradient. We end this section by comparing Corollary 1 with [34, Theorem 3.1], which provides convergence of PGD for solving a general sparsity-constrained problem. Corollary 1 reveals that the sequence generated by PGD is convergent and it converges to a stationary point of the original problem, while [34, Theorem 3.1] only shows subsequential convergence property of PGD, i.e., the limit point of any convergent subsequence converges to a stationary point.

V. SIMULATIONS

In this section, we present a set of experiments on both synthetic data and real images to illustrate the performance of the proposed method for designing sparse sensing matrices, which are compared with a set of sensing matrices designed by the existing methods [14], [15], [17], [19]. In particular, combining the dictionary Ψ (which may vary in different experiments) with different sensing matrices leads to different CS systems (Dictionary + Sensing matrix), we list below all possible CS systems that are utilized in the following experiments. We initialize Algorithm 1 with the sensing matrix given by [14, Theorem 2], but one can get similar performance with a random initialization by running slightly more iterations.

CS_{randn} :	$\Psi + \text{A dense random Gaussian matrix}$
$\text{CS}_{robsensing}$:	$\Psi + \text{Sensing matrix obtained in [15]}$
CS_{MT} :	$\Psi + \text{Sensing matrix with (15) in [17]}$
CS_{MT-ETF} :	$\Psi + \text{Sensing matrix with (16) in [17]}$
CS_{LYZCB} :	$\Psi + \text{Sensing matrix in [14]}$
$\text{CS}_{bispars}$:	$\Psi + \text{A binary sparse sensing matrix in [19]}$
$\text{CS}_{sparse-A}$:	$\Psi + \text{Output of Algorithm 1 with } \xi = 0 \text{ (i.e., } \mathcal{G}_\xi = \{\mathbf{I}\} \text{)} \text{ and } \mathbf{A} = \text{DCT}$
CS_{sparse} :	$\Psi + \text{Output of Algorithm 1 with } \xi = 0 \text{ (i.e., } \mathcal{G}_\xi = \{\mathbf{I}\} \text{)} \text{ and } \mathbf{A} = \mathbf{I}$
$\text{CS}_{sparse-ETF}$:	$\Psi + \text{Output of Algorithm 1 with } \xi = \underline{\mu} \text{ and } \mathbf{A} = \mathbf{I}$

A. Synthetic data

We generate an $N \times L$ dictionary Ψ with normally distributed entries and an $M \times N$ random matrix Φ_0 for CS_{randn} . We generate the training data as well as testing data as follows: with dictionary Ψ , first generate a set of J K -sparse $L \times 1$ vectors $\{\mathbf{s}_i\}_{i=1}^J$, where the position of the non-zero elements in \mathbf{s}_i obeys a normal distribution; then obtain sparse signals $\{\mathbf{x}_i\}_{i=1}^J$ as $\mathbf{x}_i = \Psi \mathbf{s}_i + \mathbf{e}_i$, where \mathbf{e}_i is the Gaussian noise with mean zero and covariance $\sigma^2 \mathbf{I}$. Denote SNR as the signal-to-noise ratio (in dB).

We evaluate the performance of a CS system by the mean squared error (MSE)

$$\text{MSE} \triangleq \frac{1}{N \times J} \sum_{i=1}^J \|\Psi \mathbf{s}_i - \hat{\mathbf{x}}_i\|_2^2, \quad (23)$$

where $\hat{\mathbf{x}}_i = \Psi \hat{\mathbf{s}}_i$ is the recovered signal with:

$$\hat{\mathbf{s}}_i = \arg \min_{\mathbf{s}} \|\mathbf{z}_i - \mathbf{D}\mathbf{s}\|_2^2 \quad \text{s.t. } \|\mathbf{s}\|_0 \leq K, \forall i,$$

which is solved by utilizing the OMP.

First of all, let us examine the convergence of Algorithm 1. Fig. 1 shows the evolution of the objective function $f(\Phi_k, \mathbf{G}_k)$, the iterates change $\|\Phi_{k+1} - \Phi_k\|_F$ and $\|\mathbf{G}_{k+1} - \mathbf{G}_k\|_F$, where $M = 25, N = 60, L = 80, \kappa = 20$. With similar setup, we compare the performance of different CS systems. Fig. 2 displays the relationship between signal reconstruction error MSE and SNR for all the CS systems excluding $\text{CS}_{sparse-A}$ (for synthetic data, there is no need to add any auxiliary matrix \mathbf{A}).

Remark 5.1:

- As seen from Fig. 1, the cost function $f(\Phi_k, \mathbf{G}_k)$ decays steadily and converges, the iterates change $\|\Phi_{k+1} - \Phi_k\|_F$ and $\|\mathbf{G}_{k+1} - \mathbf{G}_k\|_F$ converges to 0. This coincides with the convergence guarantee by Theorems 1 and 2. Fig. 3 displays the convergence of Algorithm 1 (which reduces to the PGD method) for solving (22) (where $\xi = 0$ and $\mathcal{G}_\xi = \{\mathbf{I}\}$). As guaranteed by Corollary 1, both the cost function $\nu(\Phi_k)$ and the iterates change $\|\Phi_{k+1} - \Phi_k\|_F$ converges.
- It is observed from Fig. 2 that CS_{MT} , CS_{MT-ETF} , CS_{sparse} and $\text{CS}_{sparse-ETF}$ outperforms the others when the sparse representation error is high. It is interesting to note that though the sensing matrices are sparse, CS_{sparse} and $\text{CS}_{sparse-ETF}$ have similar performance as CS_{MT} and CS_{MT-ETF} , and are much better than CS_{randn} and $\text{CS}_{bispars}$ (the one with a random sparse

sensing matrix). Fig. 2 also implies that CS_{MT-ETF} and $\text{CS}_{sparse-ETF}$ have respectively better performance than CS_{MT} and CS_{sparse} when SNR is high, but slightly worse when the signal has low SNR. We also observe that the performance of CS_{LYZCB} decays fast when SNR decreases; this reveals that CS_{LYZCB} is not robust to the sparse representation error. All these phenomena are also demonstrated in the experiments to be presented below using real images.

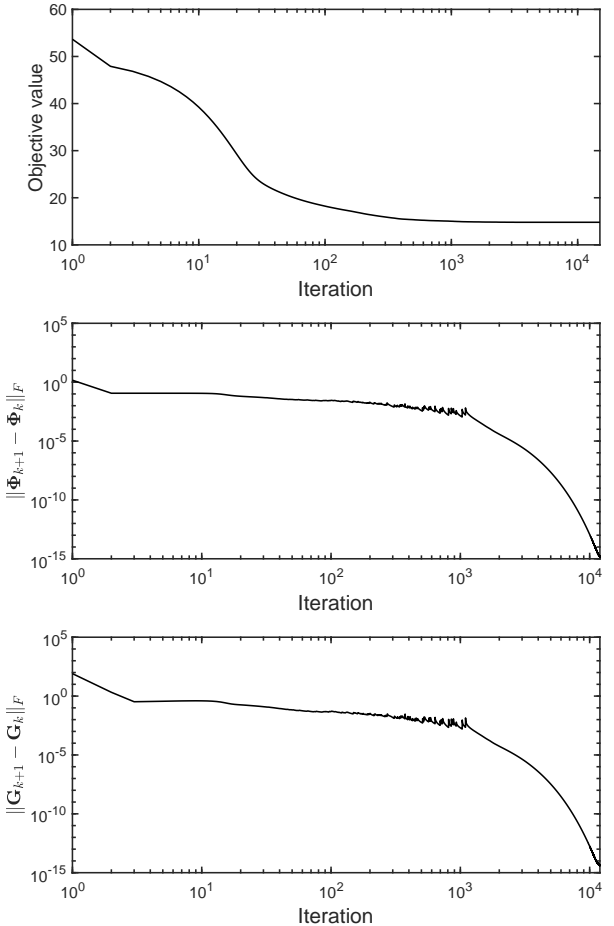


Figure 1. (upper) Evolution of the cost function $f(\Phi_k, \mathbf{G}_k)$ in (12), (middle) evolution of the iterates change $\|\Phi_{k+1} - \Phi_k\|_F$ (down) evolution of the iterates change $\|\mathbf{G}_{k+1} - \mathbf{G}_k\|_F$. Here, $M = 25, N = 60, L = 80, \lambda = 0.25$ and $\kappa = 20$.

B. Real images

In this subsection, we conduct a set of experiments on real images.⁹

We examine the performance of the CS systems with two different dictionaries: a low dimensional dictionary and a high

⁹As we stated before, compared to the sensing matrix obtained by minimizing (8) with $\xi = 0$ (i.e., $\mathcal{G}_\xi = \{\mathbf{I}\}$), the one obtained by minimizing (8) with $\xi = \underline{\mu}$ yields better performance for signals that are exactly sparse, but has worse performance for signals (like images) that are not exactly sparse under the dictionary; see also [14], [15]. Thus we only show the results for CS_{MT} and CS_{sparse} (and omit CS_{MT-ETF} and $\text{CS}_{sparse-ETF}$) on real images.

Table I
STATISTICS OF σ_{psnr} (dB) FOR SIX IMAGES PROCESSED WITH $M = 20$, $N = 64$, $L = 100$, $K = 4$, $\lambda = 1.4$ USING DIFFERENT κ .

	Lena		Couple		Barbara		Child		Plane		Man	
	$\kappa = 10$	$\kappa = 20$										
CS_{randn}	29.69	29.69	27.01	27.01	22.44	22.44	31.20	31.20	28.57	28.57	27.41	27.41
$CS_{robsensing}$	32.66	32.66	29.99	29.99	25.22	25.22	34.18	34.18	31.57	31.57	30.26	30.26
CS_{MT}	32.75	32.75	30.01	30.01	25.36	25.36	34.22	34.22	31.60	31.60	30.39	30.39
CS_{LZYCB}	12.74	12.74	10.38	10.38	4.41	4.41	15.93	15.93	14.51	14.51	9.75	9.75
$CS_{bispars}$	29.36	29.27	26.85	26.87	22.42	22.49	30.80	30.87	28.13	28.28	27.19	27.14
$CS_{sparse-A}$	32.38	32.65	29.63	29.88	24.91	25.19	33.84	34.12	31.28	31.52	30.01	30.27
CS_{sparse}	32.26	32.56	29.47	29.79	24.76	25.11	33.75	34.07	31.15	31.48	29.83	30.15

Table II
STATISTICS OF σ_{psnr} (dB) FOR SIX IMAGES PROCESSED WITH $M = 80$, $N = 256$, $L = 800$, $K = 16$, $\lambda = 0.5$ USING DIFFERENT κ .

	Lena		Couple		Barbara		Child		Plane		Man	
	$\kappa = 10$	$\kappa = 30$										
CS_{randn}	30.73	30.73	27.40	27.40	22.76	22.76	31.99	31.99	29.57	29.57	27.94	27.94
CS_{MT}	34.38	34.38	30.92	30.92	26.04	26.04	35.60	35.60	33.34	33.34	31.50	31.50
$CS_{bispars}$	30.23	30.72	27.00	27.36	22.57	22.64	31.70	31.94	29.29	29.49	27.59	27.82
$CS_{sparse-A}$	33.89	34.24	30.48	30.75	25.44	25.82	35.09	35.36	32.92	33.15	30.95	31.22
CS_{sparse}	33.17	33.50	29.69	29.94	24.26	24.60	34.38	34.66	32.41	32.61	30.06	30.39

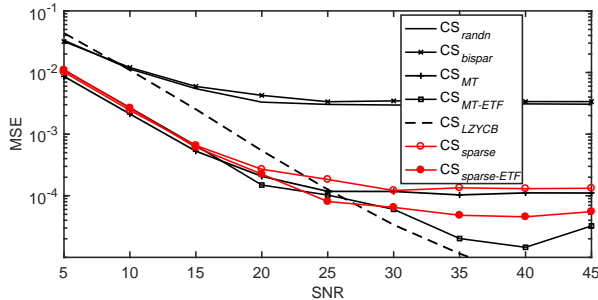


Figure 2. MSE versus input SNR. Here, $M = 25$, $N = 60$, $L = 80$, $K = 4$, $J = 2000$, $\lambda = 0.25$ and $\kappa = 20$. Disappearance from this figure means MSE is less than 10^{-5} .

dimensional dictionary. The parameters for experiments with low dimensional dictionary and high dimensional dictionary are $M = 20$, $N = 64$, $L = 100$, $K = 4$, $\lambda = 1.4$ and $M = 80$, $N = 256$, $L = 800$, $K = 16$, $\lambda = 0.5$, respectively.

We learn a low dimensional dictionary Ψ with a set of $\sqrt{N} \times \sqrt{N}$ non-overlapping patches by extracting randomly 15 patches from each of 400 images in the LabelMe [35] training data set. With each patch of $\sqrt{N} \times \sqrt{N}$ re-arranged as a vector of $N \times 1$, a set of $N \times 6000$ signals are obtained. The KSVD algorithm is conducted to learn the low dimensional dictionary [7]. Similarly, we obtain the training data for learning a high dimensional dictionary by extending the number of signal from 6000 to 10^6 and the online dictionary learning algorithm shown in [36] is utilized to learn such a high dimensional dictionary. N is set to 64 for dimensional dictionary and 256 for high dimensional dictionary.

The performance for different CS systems is evaluated by peak signal to noise ratio (PSNR), defined by

$$\text{PSNR} \triangleq 10 \times \log 10 \left[\frac{(2^r - 1)^2}{\text{MSE}} \right] (\text{dB})$$

where $r = 8$ bits per pixel and MSE is defined in (23).

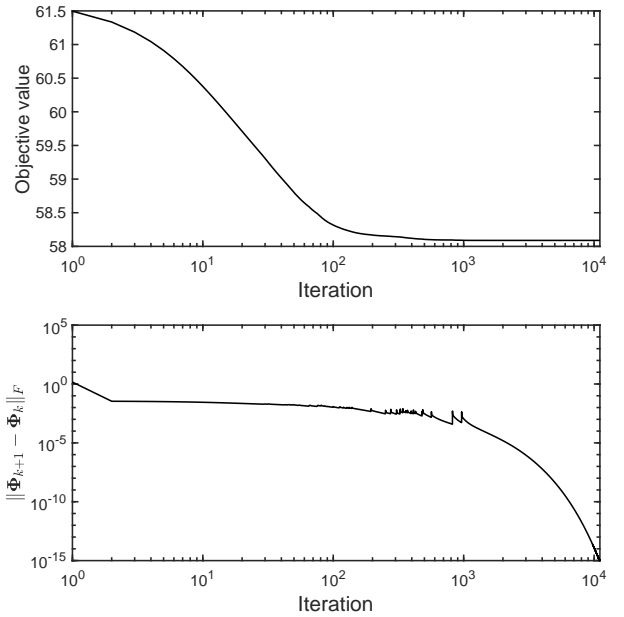


Figure 3. (upper) evolution of the cost function $\nu(\Phi_k)$ in (22), (down) evolution of the iterates change $\|\Phi_{k+1} - \Phi_k\|_F$. Here, $M = 25$, $N = 60$, $L = 80$, $\lambda = 0.25$ and $\kappa = 20$.

With image ‘‘Lena’’, we first show the PSNR versus the sparsity κ (for the sparse sensing matrices) in Fig.s 4 - 5 for the CS systems¹⁰ with a low dimensional dictionary and a high dimensional one, respectively. And furthermore, we list the performance statistics on several other images under the two settings in Tables I and II. Fig. 6 displays the visual effects of ‘‘Barbara’’.

Remark 5.2:

- As seen from Figs. 4 and 5 and aslo as expected, $CS_{sparse-A}$ and CS_{sparse} have better performance when

¹⁰Due to computational limitations, $CS_{robsensing}$ and CS_{LZYCB} are not tested for experiments with the high dimensional dictionary.

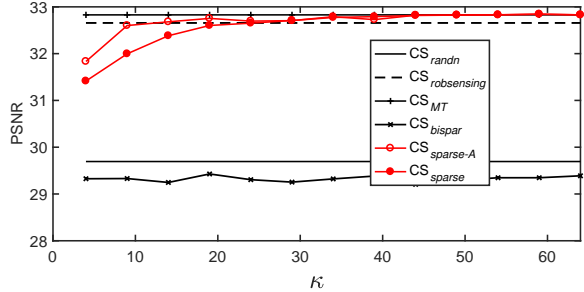


Figure 4. PSNR(dB) versus sparsity κ of sensing matrix. CS_{MT} and CS_{rands} are dense matrix. We plot it as a straight line for more convenient visual comparison. Here, $M = 20, N = 64, L = 100, K = 4, \lambda = 1.4$.

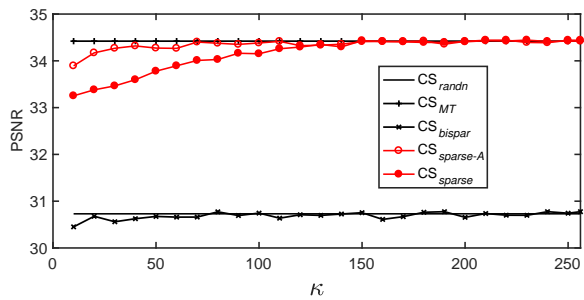


Figure 5. PSNR(dB) versus sparsity κ of sensing matrix. CS_{MT} and CS_{rands} are dense matrix. We plot it as a straight line for more convenient visual comparison. Here, $M = 80, N = 256, L = 800, K = 16, \lambda = 0.5$.

increase the sparsity κ (the number of non-zero elements in each row). However, it is surprising that even when the sparsity is very low, for example, $\kappa = 10$, $CS_{sparse-A}$ is only 0.53dB inferior to CS_{MT} , but still has more than 3dB better than CS_{rands} (which has a dense sensing matrix). We note that the gap between $CS_{sparse-A}$ and CS_{MT} is almost negligible (with 0.15 dB) when $\kappa \geq 30$ for $N = 256$ and $\kappa \geq 10$ for $N = 64$. This demonstrates our main argument that we can design a sparse sensing matrix that has similar performance as a dense matrix, but can significantly reduce the computational cost for sensing signals.

- As observed from Figs. 4 and 5 and Tables I and II, when κ is small, $CS_{sparse-A}$ has better performance than CS_{sparse} because of A . This demonstrates the effect of utilizing the auxiliary DCT matrix for structured sparse sensing matrix to increase the reconstruction accuracy. However, we note that the existence of A also increases the sensing cost in $CS_{sparse-A}$ (up to $O(N \log N)$) than the one in CS_{sparse} .
- Note that CS_{LYZCB} yields very low PSNR in Table I. This is the reason that we omit the performance of CS_{LYZCB} in Fig. 4. This (low PSNR of CS_{LYZCB}) coincides with Fig. 2 and further demonstrates that the sensing matrix in CS_{LYZCB} is not robust to the SRE. But we observe that the proposed sparse sensing matrices are robust to the error existing in sparse representation images and hence the CS_{sparse} and $CS_{sparse-A}$ have high PSNR.
- Comparing Fig. 4 with Fig. 5 (and Table I with Table II),

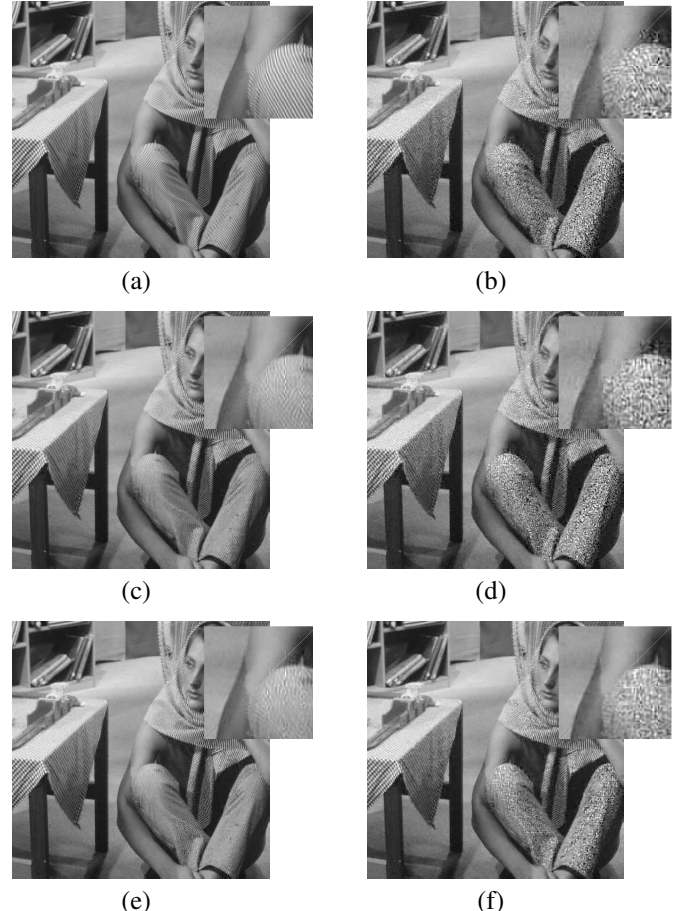


Figure 6. The original Barbara and reconstructed images from their CS samples with $M = 80, N = 256, L = 800, K = 16, \lambda = 0.5, \kappa = 10$. (a) The original one, (b) CS_{rands} , (c) CS_{MT} , (d) CS_{bispar} , (e) $CS_{sparse-A}$, and (f) CS_{sparse} .

we observe that with a high dimensional dictionary, we get high PSNR for image compression. It is of great interest to note that the proposed sparse sensing matrix is extremely useful for image compression on high dimensional patches since it can significantly reduce the computational (sampling) cost.

- Similar results are also observed for different settings of M, N, L, K . We finally note that we only compare with CS_{LYZCB} and CS_{MT} because as shown in [17] (and we also observed this), CS_{MT} has better performance than the ones in [11], [13], [15] for CS-based image compression.

VI. CONCLUSIONS

We proposed a framework for designing a structured sparse sensing matrix that is robust to sparse representation error (which widely exists in image processing) and can be efficiently implemented to capture signals. The optimal design problem is solved by an alternating minimization-based algorithm, whose convergence is rigorously analysed. The simulations demonstrate the performance of the proposed sparse sensing matrices in terms of signal reconstruction accuracy for synthetic data and PSNR for real images.

As shown in Section V, utilizing the base sensing matrix \mathbf{A} can improve the performance of the obtained sparse sensing matrix, especially when the number of non-zeros in Φ is very small. Thus, it is of interest to utilize a base sensing matrix which has a few number of degrees of freedom (or few parameters) to be optimized, making it possible to simultaneously optimize the base matrix \mathbf{A} and the sparse matrix Φ . One choice for such base sensing matrix is to utilize a series of Givens rotation matrices which have parameters for chosen and can be implemented very efficiently. We refer this to the future work.

APPENDIX A PROOF OF THEOREM 1

We first state the following definition of subdifferential for a general lower semicontinuous function, which is not necessarily differentiable.

Definition 1. (Subdifferentials [30]) Let $\sigma : \mathbb{R}^d \rightarrow (-\infty, \infty]$ be a proper and lower semicontinuous function, whose domain is defined as

$$\text{dom } \sigma := \{ \mathbf{u} \in \mathbb{R}^d : \sigma(\mathbf{u}) < \infty \}.$$

The Fréchet subdifferential $\partial_F \sigma$ of σ at \mathbf{u} is defined by

$$\partial_F \sigma(\mathbf{u}) = \left\{ \mathbf{z} : \liminf_{\mathbf{v} \rightarrow \mathbf{u}} \frac{\sigma(\mathbf{v}) - \sigma(\mathbf{u}) - \langle \mathbf{z}, \mathbf{v} - \mathbf{u} \rangle}{\|\mathbf{v} - \mathbf{u}\|} \geq 0 \right\}$$

for any $\mathbf{u} \in \text{dom } \sigma$ and $\partial_F \sigma(\mathbf{u}) = \emptyset$ if $\mathbf{u} \notin \text{dom } \sigma$.

The subdifferential $\partial \sigma(\mathbf{u})$ of σ at $\mathbf{u} \in \text{dom } \sigma$ is defined as follows

$$\partial \sigma = \{ \mathbf{z} : \exists \mathbf{u}_k \rightarrow \mathbf{u}, \sigma(\mathbf{u}_k) \rightarrow \sigma(\mathbf{u}), \mathbf{z}_k \in \partial_F \sigma(\mathbf{u}_k) \rightarrow \mathbf{z} \}$$

We say \mathbf{u} a critical point (a.k.a. stationary point) if subdifferential at \mathbf{u} is $\mathbf{0}$. The set of critical points of σ is denoted by $\mathcal{C}(\sigma)$.

Proof of Theorem 1. We prove Theorem 1 by individually proving the four arguments.

Show (P1): It is clear that for any $k \in \mathbb{N}$, $\Phi_k \in \mathcal{S}_\kappa$ and $\mathbf{G}_k \in \mathcal{G}_\xi$. Thus we have $\rho(\Phi_k, \mathbf{G}_\ell) = f(\Phi_k, \mathbf{G}_\ell)$ for any $k, \ell \in \mathbb{N}$. Let $\mathbf{B} = \Psi^T \Phi_{k+1}^T \Phi_{k+1} \Psi$. Noting that \mathcal{G}_ξ is a closed convex set, we have

$$\langle \mathbf{G} - \mathcal{P}_{\mathcal{G}_\xi}(\mathbf{B}), \mathcal{P}_{\mathcal{G}_\xi}(\mathbf{B}) - \mathbf{B} \rangle \geq 0, \quad \forall \mathbf{G} \in \mathcal{G}_\xi,$$

which directly implies

$$\begin{aligned} \rho(\Phi_{k+1}, \mathbf{G}_k) - \rho(\Phi_{k+1}, \mathbf{G}_{k+1}) &= \|\mathbf{G}_k - \mathbf{B}\|_F^2 - \|\mathbf{G}_{k+1} - \mathbf{B}\|_F^2 \\ &= \|\mathbf{G}_k - \mathcal{P}_{\mathcal{G}_\xi}(\mathbf{B}) + \mathcal{P}_{\mathcal{G}_\xi}(\mathbf{B}) - \mathbf{B}\|_F^2 - \|\mathcal{P}_{\mathcal{G}_\xi}(\mathbf{B}) - \mathbf{B}\|_F^2 \\ &= \|\mathbf{G}_k - \mathcal{P}_{\mathcal{G}_\xi}(\mathbf{B})\|_F^2 + 2 \langle \mathbf{G}_k - \mathcal{P}_{\mathcal{G}_\xi}(\mathbf{B}), \mathcal{P}_{\mathcal{G}_\xi}(\mathbf{B}) - \mathbf{B} \rangle \\ &\geq \|\mathbf{G}_k - \mathbf{G}_{k+1}\|_F^2 \geq 0. \end{aligned}$$

On the other hand, we rewrite (16) as

$$\begin{aligned} \Phi_{k+1} &\in \mathcal{P}_{\mathcal{S}_\kappa}(\Phi_k - \eta \nabla f(\Phi_k, \mathbf{G}_k)) \\ &= \underset{\mathbf{Z} \in \mathcal{S}_\kappa}{\text{argmin}} \|\mathbf{Z} - (\Phi_k - \eta \nabla f(\Phi_k, \mathbf{G}_k))\|_F^2 \\ &\in \underset{\mathbf{Z} \in \mathcal{S}_\kappa}{\text{argmin}} h_{1/\eta}(\mathbf{Z}, \Phi_k, \mathbf{G}_k) \end{aligned} \quad (24)$$

which implies that

$$\begin{aligned} h_{1/\eta}(\Phi_{k+1}, \Phi_k, \mathbf{G}_k) &\leq h_{1/\eta}(\Phi_k, \Phi_k, \mathbf{G}_k) \\ &= f(\Phi_k, \mathbf{G}_k). \end{aligned}$$

This along with Lemma 1 gives

$$\begin{aligned} f(\Phi_k, \mathbf{G}_k) - f(\Phi_{k+1}, \mathbf{G}_k) &\geq f(\Phi_k, \mathbf{G}_k) - h_{L_c}(\Phi_{k+1}, \Phi_k, \mathbf{G}_k) \\ &\geq h_{1/\eta}(\Phi_{k+1}, \Phi_k, \mathbf{G}_k) - h_{L_c}(\Phi_{k+1}, \Phi_k, \mathbf{G}_k) \\ &= \frac{1}{\eta} - L_c \|\Phi_k - \Phi_{k+1}\|_F^2. \end{aligned}$$

Show (P2): It follows from (19) that

$$\begin{aligned} \rho_0 &\geq \rho(\Phi_1, \mathbf{G}_0) \geq \rho(\Phi_1, \mathbf{G}_1) \geq \cdots \rho(\Phi_k, \mathbf{G}_k) \\ &\geq \rho(\Phi_{k+1}, \mathbf{G}_k) \geq \rho(\Phi_{k+1}, \mathbf{G}_{k+1}) \geq \cdots \end{aligned}$$

which together with the fact that $\rho(\Phi_k, \Psi_k) \geq 0$ gives the convergence of sequence $\{\rho(\Phi_k, \mathbf{G}_k)\}_{k \geq 0}$. This also implies that $(\Phi_k, \mathbf{G}_k) \in \mathcal{L}_{\rho_0}$ and hence $\{(\Phi_k, \mathbf{G}_k)\}_{k \geq 0}$ is a bounded sequence.

Show (P3): Utilizing (19) for all $k \in \mathbb{N}$ and summing them together, we obtain

$$\begin{aligned} \sum_{k=0}^{\infty} \frac{1}{\eta} - L_c (\|\Phi^k - \Phi^{k+1}\|_F^2) + \|\mathbf{G}^k - \mathbf{G}^{k+1}\|_F^2 \\ \leq \rho_0 - \lim_{k \rightarrow \infty} \rho(\Phi_k, \mathbf{G}_k) \leq \rho_0, \end{aligned}$$

which implies that the series $\{\sum_{k=0}^n \|\Phi^k - \Phi^{k+1}\|_F^2 + \|\mathbf{G}^k - \mathbf{G}^{k+1}\|_F^2\}_n$ is convergent. This together with the fact that $\|\Phi^k - \Phi^{k+1}\|_F^2 \geq 0$ and $\|\mathbf{G}^k - \mathbf{G}^{k+1}\|_F^2 \geq 0$ gives (20).

Show (P4): We rewrite (24) as

$$\Phi_{k+1} \in \underset{\Phi \in \mathbb{R}^{M \times N}}{\text{argmin}} h_{\frac{1}{\eta}}(\Phi, \Phi_k, \mathbf{G}_k) + \delta_{\mathcal{S}_\kappa}(\Phi), \quad (25)$$

which implies (by the optimality of Φ_{k+1} in (25) and letting $\Phi = \underline{\Phi}$, i.e. the limit of a convergent subsequence $\{\Phi_{k'}\}_{k'}$)

$$\begin{aligned} \langle \nabla_{\Phi} f(\Phi_k, \mathbf{G}_k), \Phi_{k+1} - \Phi_k \rangle + \frac{\eta}{2} \|\Phi_{k+1} - \Phi_k\|_F^2 + \delta_{\mathcal{S}_\kappa}(\Phi_{k+1}) \\ \leq \langle \nabla_{\Phi} f(\Phi_k, \mathbf{G}_k), \underline{\Phi} - \Phi_k \rangle + \frac{\eta}{2} \|\underline{\Phi} - \Phi_k\|_F^2 + \delta_{\mathcal{S}_\kappa}(\underline{\Phi}). \end{aligned}$$

This further gives (take limit on subsequence $\{\Phi_{k'}\}_{k'}$)

$$\begin{aligned} \limsup_{k' \rightarrow \infty} \delta_{\mathcal{S}_\kappa}(\Phi_{k'}) - \delta_{\mathcal{S}_\kappa}(\underline{\Phi}) &\leq \limsup_{k' \rightarrow \infty} \langle \nabla_{\Phi} f(\Phi_{k'-1}, \mathbf{G}_{k'-1}), \underline{\Phi} - \Phi_{k'} \rangle \\ &\quad + \frac{\eta}{2} \|\Phi_{k'-1} - \underline{\Phi}\|_F^2 - \frac{\eta}{2} \|\Phi_{k'} - \Phi_{k'-1}\|_F^2 \\ &= 0, \end{aligned} \quad (26)$$

where the last line follows from (20), the fact that scalar product is continuous and $\lim_{k' \rightarrow \infty} \|\Phi_{k'-1} - \underline{\Phi}\|_F = 0$ since

$$\begin{aligned} 0 &\leq \lim_{k' \rightarrow \infty} \|\Phi_{k'-1} - \underline{\Phi}\|_F \\ &= \lim_{k' \rightarrow \infty} \|\Phi_{k'-1} - \Phi_{k'} + \Phi_{k'} - \underline{\Phi}\|_F \\ &\leq \lim_{k' \rightarrow \infty} \|\Phi_{k'} - \underline{\Phi}\|_F + \|\Phi_{k'} - \Phi_{k'-1}\|_F = 0. \end{aligned}$$

From the fact that $\delta_{\mathcal{S}_\kappa}(\underline{\Phi})$ is lower semi-continuous, we have

$$\delta_{\mathcal{S}_\kappa}(\underline{\Phi}) \leq \liminf_{k' \rightarrow \infty} \delta_{\mathcal{S}_\kappa}(\Phi_{k'}).$$

Utilizing (26) gives

$$\limsup_{k' \rightarrow \infty} \delta_{\mathcal{S}_\kappa}(\Phi_{k'}) \leq \delta_{\mathcal{S}_\kappa}(\underline{\Phi}) \leq \liminf_{k' \rightarrow \infty} \delta_{\mathcal{S}_\kappa}(\Phi_{k'}),$$

which together with the fact $\liminf_{k' \rightarrow \infty} \delta_{\mathcal{S}_\kappa}(\Phi_{k'}) \leq \limsup_{k' \rightarrow \infty} \delta_{\mathcal{S}_\kappa}(\Phi_{k'})$ gives

$$\delta_{\mathcal{S}_\kappa}(\underline{\Phi}) = \liminf_{k' \rightarrow \infty} \delta_{\mathcal{S}_\kappa}(\Phi_{k'}) = \limsup_{k' \rightarrow \infty} \delta_{\mathcal{S}_\kappa}(\Phi_{k'}),$$

and hence

$$\lim_{k' \rightarrow \infty} \delta_{\mathcal{S}_\kappa}(\Phi_{k'}) = \delta_{\mathcal{S}_\kappa}(\underline{\Phi}).$$

Since \mathcal{G}_ξ is a compact set and $\mathbf{G}_{k'} \in \mathcal{G}_\xi$, $\forall k' \in \mathbb{N}$, we have the limit point $\underline{\mathbf{G}} \in \mathcal{G}_\xi$. Therefore, we obtain

$$\begin{aligned} \lim_{k' \rightarrow \infty} \rho(\Phi_{k'}, \mathbf{G}_{k'}) &= \lim_{k' \rightarrow \infty} f(\Phi_{k'}, \mathbf{G}_{k'}) + \delta_{\mathcal{S}_\kappa}(\Phi_{k'}) + \delta_{\mathcal{G}_\xi}(\mathbf{G}_{k'}) \\ &= \rho(\underline{\Phi}, \underline{\mathbf{G}}). \end{aligned}$$

The remaining part is to prove that $\underline{\mathbf{W}} = (\underline{\Phi}, \underline{\mathbf{G}})$ is a stationary point of ρ , which is equivalent to show $(\mathbf{0}, \mathbf{0}) \in \partial\rho(\underline{\Phi}, \underline{\mathbf{G}})$. In what follows, we show a stronger result that $(\mathbf{0}, \mathbf{0}) \in \lim_{k \rightarrow \infty} \partial\rho(\Phi_k, \mathbf{G}_k)$.

First note that

$$\mathbf{G}_k = \underset{\mathbf{G} \in \mathbb{R}^{L \times L}}{\operatorname{argmin}} \rho(\Phi_k, \mathbf{G})$$

The optimality condition gives

$$\mathbf{0} = \underbrace{\nabla_{\mathbf{G}} f(\Phi_k, \mathbf{G}_k) + \mathbf{U}_k}_{\mathbf{D}_{\mathbf{G}_k}} \in \partial_{\mathbf{G}} \rho(\mathbf{W}_k), \quad (27)$$

where $\mathbf{U}_k \in \partial\delta_{\mathcal{G}_\xi}(\mathbf{G}_k)$. On the other hand, the optimality condition of (25) gives (by setting $k = k - 1$ in (25))

$$\nabla_{\Phi} f(\Phi_{k-1}, \mathbf{G}_{k-1}) + \frac{1}{\eta}(\Phi_k - \Phi_{k-1}) + \mathbf{V}_k = \mathbf{0},$$

where $\mathbf{V}_k \in \partial\delta_{\mathcal{S}_\kappa}(\Phi_k)$. Thus we have

$$\underbrace{\nabla_{\Phi} f(\mathbf{W}_k) - \nabla_{\Phi} f(\mathbf{W}_{k-1}) - \frac{1}{\eta}(\Phi_k - \Phi_{k-1})}_{\mathbf{D}_{\Phi_k}} \in \partial_{\Phi} \rho(\mathbf{W}_k),$$

which along with (27) gives

$$\begin{aligned} \|\mathbf{D}_{\Phi_k}, \mathbf{D}_{\mathbf{G}_k}\|_F &= \|\mathbf{D}_{\Phi_k}\|_F \\ &= \|\nabla_{\Phi} f(\mathbf{W}_k) - \nabla_{\Phi} f(\mathbf{W}_{k-1}) - \frac{1}{\eta}(\Phi_k - \Phi_{k-1})\|_F \\ &\leq \|\nabla_{\Phi} f(\mathbf{W}_k) - \nabla_{\Phi} f(\Phi_k, \mathbf{G}_{k-1})\| \\ &\quad + \|\nabla_{\Phi} f(\Phi_k, \mathbf{G}_{k-1}) - \nabla_{\Phi} f(\mathbf{W}_{k-1})\| \\ &\quad + \frac{1}{\eta}\|\Phi_k - \Phi_{k-1}\|_F \\ &\leq L_c \|\mathbf{G}_k - \mathbf{G}_{k-1}\|_F + (L_c + \frac{1}{\eta})\|\Phi_k - \Phi_{k-1}\|_F \\ &\leq (2L_c + \frac{1}{\eta})\|\mathbf{W}_k - \mathbf{W}_{k-1}\|_F, \end{aligned} \quad (28)$$

where we have used the Lipschitz gradient (18) in the second inequality.

Applying (20), we finally obtain

$$\lim_{k \rightarrow \infty} (\mathbf{D}_{\Phi_k}, \mathbf{D}_{\mathbf{G}_k}) = (\mathbf{0}, \mathbf{0})$$

since

$$\lim_{k \rightarrow \infty} \|(\mathbf{D}_{\Phi_k}, \mathbf{D}_{\mathbf{G}_k})\|_F = 0.$$

Thus $(\mathbf{0}, \mathbf{0}) \in \lim_{k \rightarrow \infty} \partial\rho(\Phi_k, \mathbf{G}_k)$ and we conclude that any convergent subsequence of $\{\mathbf{W}_k\}$ converges to a stationary point of (17).

Finally, the statement

$$\lim_{k \rightarrow \infty} \rho(\mathbf{W}_k) = \rho(\underline{\mathbf{W}}).$$

directly follows from (P2) that the objective value sequence $\{\rho(\mathbf{W}_k)\}_{k \in \mathbb{N}}$ is convergent. \square

APPENDIX B PROOF OF THEOREM 2

We first state the definition of Kurdyka-Łojasiewicz (KL) inequality, which is proved to be useful for convergence analysis [30]–[32].

Definition 2. A proper semi-continuous function $\sigma(\mathbf{u})$ is said to satisfy Kurdyka-Łojasiewicz (KL) inequality, if $\underline{\mathbf{u}}$ is a stationary point of $\sigma(\mathbf{u})$, then $\exists \delta > 0$, $\theta \in [0, 1)$, $C_1 > 0$, s.t.

$$|\sigma(\mathbf{u}) - \sigma(\underline{\mathbf{u}})|^\theta \leq C_1 \|\mathbf{v}\|, \quad \forall \mathbf{u} \in B(\underline{\mathbf{u}}, \delta), \quad \forall \mathbf{v} \in \partial\sigma(\mathbf{u})$$

It is clear that our objective function $\rho(\Phi, \mathbf{G})$ is lower semi-continuous and it satisfies the above KL inequality since the three components $f(\Phi, \mathbf{G})$, $\delta_{\mathcal{S}_\kappa}(\Phi)$ and $\delta_{\mathcal{G}_\xi}(\mathbf{G})$ all have the KL inequality [31], [32].

Proof of Theorem 2. theorem 1 reveals the subsequential convergence property of the iterates sequence $\{\mathbf{W}_k = (\Phi_k, \mathbf{G}_k)\}_k$, i.e., the limit point of any convergent subsequence converges to a stationary point. In what follows, we show the sequence $\{\mathbf{W}_k = (\Phi_k, \mathbf{G}_k)\}_k$ itself is indeed convergent, and hence it converges to a certain stationary point of $\underline{\mathbf{W}} = (\underline{\Phi}, \underline{\mathbf{G}})$.

It follows from (21) that for any $\delta > 0$, there exists an integer n such that $\mathbf{W}_k \in B(\underline{\mathbf{W}}, \delta)$, $\forall k > n$ for some stationary point $\underline{\mathbf{W}} \in \mathcal{C}(\rho)$. From the concavity of the function $h(y) = y^{1-\theta}$ with domain $y > 0$, we have¹¹

$$\begin{aligned} &[\rho(\mathbf{W}_{k+1}) - \rho(\underline{\mathbf{W}})]^{1-\theta} \\ &\leq [\rho(\mathbf{W}_k) - \rho(\underline{\mathbf{W}})]^{1-\theta} + (1-\theta) \frac{\rho(\mathbf{W}_{k+1}) - \rho(\mathbf{W}_k)}{[\rho(\mathbf{W}_k) - \rho(\underline{\mathbf{W}})]^\theta}. \end{aligned} \quad (29)$$

We now provide lower bound and upper bound for $\rho(\mathbf{W}_k) - \rho(\mathbf{W}_{k+1})$ and $[\rho(\mathbf{W}_k) - \rho(\underline{\mathbf{W}})]^\theta$, respectively. It follows from (19) that

$$\rho(\mathbf{W}_k) - \rho(\mathbf{W}_{k+1}) \geq C_2 \|\mathbf{W}_{k+1} - \mathbf{W}_k\|_F^2,$$

where $C_2 = \min\{\frac{1}{2} - L_c, 1\}$. On the other hand, from (28) and the KL inequality we have

$$\begin{aligned} &[\rho(\mathbf{W}_k) - \rho(\underline{\mathbf{W}})]^\theta \leq C_1 \|(\mathbf{D}_{\Phi_k}, \mathbf{D}_{\mathbf{G}_k})\|_F \\ &\leq C_3 \|\mathbf{W}_k - \mathbf{W}_{k-1}\|_F, \end{aligned}$$

¹¹If a differential function $f(\mathbf{x})$ is concavity, the following inequality holds: $f(\mathbf{y}) - f(\mathbf{x}) \leq \langle \nabla f(\mathbf{x}), \mathbf{y} - \mathbf{x} \rangle$.

where $C_3 = C_1(2L_c + 1/\eta)$. Plugging the above two inequalities into (29) gives

$$\begin{aligned} & [\rho(\mathbf{W}_k) - \rho(\underline{\mathbf{W}})]^{1-\theta} - [\rho(\mathbf{W}_{k+1}) - \rho(\underline{\mathbf{W}})]^{1-\theta} \\ & \geq (1-\theta) \frac{C_2 \|\mathbf{W}_{k+1} - \mathbf{W}_k\|_F^2}{C_3 \|\mathbf{W}_k - \mathbf{W}_{k-1}\|_F}. \end{aligned} \quad (30)$$

Let $C_4 = (1-\theta)C_2/C_3$. Repeating the above equation for k from 1 to ∞ and summing them gives

$$\begin{aligned} & \frac{1}{C_4} [\rho(\mathbf{W}_1) - \rho(\underline{\mathbf{W}})]^{1-\theta} - \frac{1}{C_4} [\rho(\mathbf{W}_\infty) - \rho(\underline{\mathbf{W}})]^{1-\theta} \\ & \geq \sum_{k=1}^{\infty} \frac{\|\mathbf{W}_{k+1} - \mathbf{W}_k\|_F^2}{\|\mathbf{W}_k - \mathbf{W}_{k-1}\|_F} + \|\mathbf{W}_k - \mathbf{W}_{k-1}\|_F \\ & \quad - \|\mathbf{W}_k - \mathbf{W}_{k-1}\|_F \\ & \stackrel{(i)}{\geq} 2 \sum_{k=1}^{\infty} \|\mathbf{W}_{k+1} - \mathbf{W}_k\|_F - \sum_{k=1}^{\infty} \|\mathbf{W}_k - \mathbf{W}_{k-1}\|_F \\ & = \sum_{k=1}^{\infty} \|\mathbf{W}_{k+1} - \mathbf{W}_k\|_F - \|\mathbf{W}_1 - \mathbf{W}_0\|_F \end{aligned}$$

where (i) is from the arithmetic inequality, i.e., $a^2 + b^2 \geq 2ab$. The proof is completed by applying the above result with the boundedness of $\{\mathbf{W}_k\}_k$ and (21):

$$\sum_{k=1}^{\infty} \|\mathbf{W}_{k+1} - \mathbf{W}_k\|_F < \infty$$

which implies that the sequence $\{\mathbf{W}_k\}_{k \in \mathbb{N}}$ is Cauchy [32] in a compact set and hence it is convergent. \square

APPENDIX C

THE CHOICE OF STEP SIZE WITH UNKNOWN LIPSCHITZ CONSTANT L_c

In practice, it is of challenge to choose an appropriate step size since it is not easy to compute the Lipschitz constant L_c in some cases. Fortunately, according to the given convergence analysis in Section IV, we know if the step size is chosen satisfying (19), the convergence is still guaranteed. Thus, we utilize the backtracking method with inequality (19) to search an appropriate step size without knowing the Lipschitz constant L_c . The procedure is detailed in Algorithm 2.

Algorithm 2 Backtracking Procedure

Initialization:

Initial value: (η_0, γ, α) where η_0 is the initial guess step size, $\gamma \in (0, 1)$ and $\alpha \in (0, 1)$.

Output:

Step size η and Updated Φ_{k+1} .

- 1: $\eta \leftarrow \eta_0$
- 2: $\Phi_{k+1} \leftarrow \mathcal{P}_{\mathcal{S}_\kappa}(\Phi_k - \eta \nabla_{\Phi} f(\Phi_k, \mathbf{G}_k))$
- 3: **while** $\rho(\Phi_k, \mathbf{G}_k) - \rho(\Phi_{k+1}, \mathbf{G}_k) < \frac{\gamma}{2\eta} \|\Phi_{k+1} - \Phi_k\|_F^2$ **do**
- 4: $\eta \leftarrow \alpha\eta$
- 5: Update Φ_{k+1} : $\Phi_{k+1} \leftarrow \mathcal{P}_{\mathcal{S}_\kappa}(\Phi_k - \eta \nabla_{\Phi} f(\Phi_k, \mathbf{G}_k))$
- 6: **end while**

REFERENCES

- [1] E. Candès, J. Romberg, and T. Tao, "Robust uncertainty principles: Exact signal reconstruction from highly incomplete frequency information," *IEEE Trans. Inf. Theory*, vol. 52, no. 2, pp. 489–509, 2006.
- [2] E. Candès and M. B. Wakin, "An introduction to compressive sampling," *IEEE Signal Process. Mag.*, vol. 25, no. 2, pp. 21–30, 2008.
- [3] E. J. Candès, J. K. Romberg, and T. Tao, "Stable signal recovery from incomplete and inaccurate measurements," *Commun. Pure Appl. Math.*, vol. 59, no. 8, pp. 1207–1223, 2006.
- [4] D. L. Donoho, "Compressed sensing," *IEEE Trans. Inf. Theory*, vol. 52, no. 4, pp. 1289–1306, 2006.
- [5] Z. Zhu and M. B. Wakin, "Approximating sampled sinusoids and multiband signals using multiband modulated DPSS dictionaries," to appear in *J. Fourier Anal. Appl.*
- [6] K. Engan, S. O. Aase, and J. Hakon Husoy, "Method of optimal directions for frame design," in *Proc. IEEE Int. Conf. Acoust., Speech, and Signal Processing (ICASSP)*, vol. 5, pp. 2443–2446, 1999.
- [7] M. Aharon, M. Elad, and A. Bruckstein, "K-SVD: An algorithm for designing overcomplete dictionaries for sparse representation," *IEEE Trans. Signal Process.*, vol. 54, no. 11, pp. 4311–4322, 2006.
- [8] G. Li, Z. Zhu, H. Bai, and A. Yu, "A new framework for designing incoherent sparsifying dictionaries," in *IEE Int. Conf. Acous. Speech, Signal Process. (ICASSP)*, pp. 4416–4420, IEEE, 2017.
- [9] R. Baraniuk, M. Davenport, R. DeVore, and M. Wakin, "A simple proof of the restricted isometry property for random matrices," *Constructive Approx.*, vol. 28, no. 3, pp. 253–263, 2008.
- [10] A. S. Bandeira, E. Dobriban, D. G. Mixon, and W. F. Sawin, "Certifying the restricted isometry property is hard," *IEEE Trans. Inf. Theory*, vol. 59, no. 6, pp. 3448–3450, 2013.
- [11] M. Elad, "Optimized projections for compressed sensing," *IEEE Trans. Signal Process.*, vol. 55, no. 12, pp. 5695–5702, 2007.
- [12] J. M. Duarte-Carvajalino and G. Sapiro, "Learning to sense sparse signals: Simultaneous sensing matrix and sparsifying dictionary optimization," *IEEE Trans. Image Process.*, vol. 18, no. 7, pp. 1395–1408, 2009.
- [13] V. Abolghasemi, S. Ferdowsi, and S. Sanei, "A gradient-based alternating minimization approach for optimization of the measurement matrix in compressive sensing," *Signal Process.*, vol. 92, no. 4, pp. 999–1009, 2012.
- [14] G. Li, Z. Zhu, D. Yang, L. Chang, and H. Bai, "On projection matrix optimization for compressive sensing systems," *IEEE Trans. Signal Process.*, vol. 61, no. 11, pp. 2887–2898, 2013.
- [15] G. Li, X. Li, S. Li, H. Bai, Q. Jiang, and X. He, "Designing robust sensing matrix for image compression," *IEEE Trans. Image Process.*, vol. 24, no. 12, pp. 5389–5400, 2015.
- [16] T. Hong, H. Bai, S. Li, and Z. Zhu, "An efficient algorithm for designing projection matrix in compressive sensing based on alternating optimization," *Signal Process.*, vol. 125, pp. 9–20, 2016.
- [17] T. Hong and Z. Zhu, "An efficient method for robust projection matrix design," *Signal Process.*, vol. 143, no. 3, pp. 200–210, 2018.
- [18] F. Chen, A. P. Chandrakasan, and V. M. Stojanovic, "Design and analysis of a hardware-efficient compressed sensing architecture for data compression in wireless sensors," *IEEE J. Solid-State Circuits*, vol. 47, no. 3, pp. 744–756, 2012.
- [19] H. Mamaghani, N. Khaled, D. Atienza, and P. Vandergheynst, "Compressed sensing for real-time energy-efficient ecg compression on wireless body sensor nodes," *IEEE T. Biom. Engineer.*, vol. 58, no. 9, pp. 2456–2466, 2011.
- [20] A. Gilbert and P. Indyk, "Sparse recovery using sparse matrices," *Proceedings of the IEEE*, vol. 98, no. 6, pp. 937–947, 2010.
- [21] T. Strohmer and R. W. Heath, "Grassmannian frames with applications to coding and communication," *Appl. Comput. Harmon. Anal.*, vol. 14, no. 3, pp. 257–275, 2003.
- [22] S. S. Chen, D. L. Donoho, and M. A. Saunders, "Atomic decomposition by basis pursuit," *SIAM J. Sci. Comput.*, vol. 20, no. 1, pp. 33–61, 1998.
- [23] D. L. Donoho and M. Elad, "Optimally sparse representation in general (nonorthogonal) dictionaries via l_1 minimization," *Proc. Natt. Acad. Sci.*, vol. 100, no. 5, pp. 2197–2202, 2003.
- [24] J. A. Tropp, "Greed is good: Algorithmic results for sparse approximation," *IEEE Trans. Inf. Theory*, vol. 50, no. 10, pp. 2231–2242, 2004.
- [25] J. Sulam, B. Ophir, M. Zibulevsky, and M. Elad, "Trainlets: Dictionary learning in high dimensions," *IEEE Transactions on Signal Processing*, vol. 64, no. 12, pp. 3180–3193, 2016.
- [26] R. Rubinstein, M. Zibulevsky, and M. Elad, "Double sparsity: Learning sparse dictionaries for sparse signal approximation," *IEEE Trans. Signal Process.*, vol. 58, no. 3, pp. 1553–1564, 2010.

- [27] P. Dita, “Factorization of unitary matrices,” *Journal of Physics A: Mathematical and General*, vol. 36, no. 11, p. 2781, 2003.
- [28] Z. Zhu, Q. Li, G. Tang, and M. B. Wakin, “Global optimality in low-rank matrix optimization,” *arXiv preprint arXiv:1702.07945*, 2017.
- [29] Q. Li and G. Tang, “The nonconvex geometry of low-rank matrix optimizations with general objective functions,” *arXiv preprint arXiv:1611.03060*, 2016.
- [30] H. Attouch, J. Bolte, P. Redont, and A. Soubeiran, “Proximal alternating minimization and projection methods for nonconvex problems: An approach based on the kurdyka–lojasiewicz inequality,” *Mathematics of Operations Research*, vol. 35, no. 2, pp. 438–457, 2010.
- [31] H. Attouch, J. Bolte, and B. F. Svaiter, “Convergence of descent methods for semi-algebraic and tame problems: proximal algorithms, forward–backward splitting, and regularized gauss–seidel methods,” *Math. Program.*, vol. 137, no. 1-2, pp. 91–129, 2013.
- [32] J. Bolte, S. Sabach, and M. Teboulle, “Proximal alternating linearized minimization for nonconvex and nonsmooth problems,” *Math. Program.*, vol. 146, no. 1-2, pp. 459–494, 2014.
- [33] T. Blumensath and M. E. Davies, “Iterative hard thresholding for compressed sensing,” *Applied and computational harmonic analysis*, vol. 27, no. 3, pp. 265–274, 2009.
- [34] A. Beck and Y. C. Eldar, “Sparsity constrained nonlinear optimization: Optimality conditions and algorithms,” *SIAM J. Optimiz.*, vol. 23, no. 3, pp. 1480–1509, 2013.
- [35] B. C. Russell, A. Torralba, K. P. Murphy, and W. T. Freeman, “Labelme: a database and web-based tool for image annotation,” *Int. J. Computer Vision*, vol. 77, no. 1, pp. 157–173, 2008.
- [36] J. Mairal, F. Bach, J. Ponce, and G. Sapiro, “Online dictionary learning for sparse coding,” in *Proc. the 26th ann. int. conf. machine learning(ICML)*, pp. 689–696, ACM, 2009.